arXiv:2301.02460v2 [cond-mat.mes-hall] 18 Apr 2023

Half-metal and other fractional metal phases in doped AB bilayer graphene

A.L. Rakhmanov,[1] A.V. Rozhkov,[1] A.O. Sboychakov,[1] and Franco Nori[2,3]

[1] *Institute for Theoretical and Applied Electrodynamics, Russian Academy of Sciences, 125412 Moscow, Russia*

[2] *Center for Quantum Computing and Cluster for Pioneering Research, RIKEN, Wako-shi, Saitama, 351-0198, Japan*

[3] *Department of Physics, University of Michigan, Ann Arbor, MI 48109-1040, USA*

(Dated: April 19, 2023)

We theoretically argue that, in doped AB bilayer graphene, the electron-electron coupling can give rise to the spontaneous formation of fractional metal phases. These states, being generalizations of a more common half-metal, have a Fermi surface that is perfectly polarized not only in terms of a spin-related quantum number, but also in terms of the valley index. The proposed mechanism assumes that the ground state of undoped bilayer graphene is a spin density wave insulator, with a finite gap in the single-electron spectrum. Upon doping, the insulator is destroyed, and replaced by a fractional metal phase. As doping increases, transitions between various types of fractional metal (half-metal, quarter-metal, etc.) are triggered. Our findings are consistent with recent experiments on doped AB bilayer graphene, in which a cascade of phase transitions between different isospin states was observed.

PACS numbers: 73.22.Pr, 73.22.Gk

I. INTRODUCTION

A usual metal demonstrates perfect symmetry with regard to the carriers' spin projection. This symmetry manifests itself in the vanishing total spin magnetization and the Fermi-surface spin degeneracy. Yet the symmetry can be spontaneously destroyed by sufficiently strong electron-electron interaction, which may result, for example, in the formation of two non-identical Fermi surfaces for the two spin projections. In the extreme case of the so-called half-metals (HM), one of these projections is completely absent from the Fermi surface, while all states at the Fermi energy have identical spin quantum number[1–3]. Various rather dissimilar materials with transition-metal atoms are found to be half-metals[4–7]. Several papers[8–12] predicted the half-metallicity in carbon-based systems as well. The existence of spin-polarized currents in such systems makes them promising materials for applications in spintronics[3,13].

Graphene-based bilayer and multi-layer systems posses additional quantum number, the valley index. In these materials, besides the spin-related polarization, a many-body state may demonstrate a valley polarization. Therefore, for graphene-based materials, the notion of a HM can be generalized to include the possibility of a Fermi surface with perfect valley polarization as well. Such a proposal was put forward in Ref. 14, where the concept of a quarter-metal (QM) was formulated. A Fermi surface of a QM state is perfectly polarized both in valley and in spin-related indices. Furthermore, the latter paper explained that both an HM and a QM should be viewed as specific instances of a more general notion, 'a fractional metal' (FraM). This many-body phase may be realized in materials with degenerate Fermi surface. The higher the degeneracy, the stronger fractionalization of the Fermi surface can be achieved.

Since our publication[14] the experimental observation of a QM state in graphene trilayer has been claimed[15]. The experimental data of Ref. 16 suggest that a QM and FraM states can be stabilized in a sample of AB bilayer graphene (AB-BLG). Given these experimental successes it appears important to develop a microscopic theoretical framework that can explain the existence of the FraM in the AB-BLG. In this paper, a suitable mechanism is proposed and discussed.

II. MODEL

An elementary unit cell of the AB-BLG consists of four atoms (sublattices A and B, and layers 1 and 2) with the distance between neighboring carbon atoms $a_0 \approx 0.142\,\text{nm}$ and interlayer distance $c_0 \approx 0.335\,\text{nm}$. The hoping amplitude t connecting the nearest A and B sites in the layer is $2.5\,\text{eV} \lesssim t \lesssim 3\,\text{eV}$. The hopping between the nearest sites in different layers can be estimated as $0.3\,\text{eV} \lesssim t_0 \lesssim 0.4\,\text{eV}$. It is possible to introduce additional, longer-range, hopping amplitudes into the model. We assume, however, that the effect of these amplitudes is weak, and they are neglected.

The AB-BLG Brillouin zone is a regular hexagon, with two non-equivalent Dirac points at

$$\mathbf{K}_1 = \frac{2\pi}{3\sqrt{3}a_0}(\sqrt{3},1) \quad \text{and} \quad \mathbf{K}_2 = \frac{2\pi}{3\sqrt{3}a_0}(\sqrt{3},-1). \tag{1}$$

It is convenient to measure momentum relative to the Dirac points. Thus, we introduce $\mathbf{q} = \mathbf{k} - \mathbf{K}_{1,2}$.

The energy spectrum of undoped AB-BLG consists of four bands, two electron and two hole ones. Since we are interested in the low-energy spectrum of AB-BLG, $q \ll 2t_0/3ta_0$, we restrict our consideration to the effective two-band model. It has one electron and one hole band, both bands have quadratic dispersion. The bands touch

at the Fermi energy. When the (small) trigonal warping terms are ignored, the Hamiltonian for a single-electron wave function reads[17–19]

$$H_0 = -\frac{\hbar^2 v_{\rm F}^2}{t_0}\begin{pmatrix} 0 & (iq_x+\xi q_y)^2 \\ (iq_x-\xi q_y)^2 & 0 \end{pmatrix}, \quad (2)$$

where the graphene Fermi velocity is $v_{\rm F} = 3a_0 t/2\hbar$ and ξ is the valley index. The value $\xi = 1$ corresponds to $\mathbf{K}_1$ and $\xi = -1$ corresponds to $\mathbf{K}_2$. In the second-quantization formalism we can write

$$H_0 = \sum_{\mathbf{q}\sigma\xi l} \varepsilon_{\mathbf{q}l}\gamma^\dagger_{\mathbf{q}l\sigma\xi}\gamma_{\mathbf{q}l\sigma\xi}, \quad (3)$$

where the spin projection is denoted by σ, the index l labels the electron ($l = 1$) or hole ($l = 2$) band, and $\gamma_{\mathbf{q}l\sigma\xi}$ is the corresponding second quantization operator. The eigenenergies $\varepsilon_{\mathbf{q}l}$ of the Hamiltonian (2) are

$$\varepsilon_{\mathbf{q}l} = (-1)^{l+1}\frac{\hbar^2 v_{\rm F}^2}{t_0}q^2. \quad (4)$$

Next we include the electron-electron repulsion into the model. The latter is a highly non-trivial task. Clearly, the low-energy two-band effective model (2) is incompatible with the bare Coulomb repulsion. Instead, an effective interaction Hamiltonian must be derived. Unfortunately, a compact description of such an effective interaction remains an elusive theoretical goal. Indeed, due to multiple factors affecting the many-body physics in graphene and graphene-based systems, an effective interaction term is quite complex, with multiple coupling constants, whose non-universal values are poorly known[20–24]. In this situation we prefer to adopt a semi-phenomenological approach, keeping only the terms that directly contribute to the spin-density wave (SDW) ordering. It is possible to identify three types of such terms. The first term arises due to the forward-scattering

$$H^{\rm f}_{\rm int} = \frac{V_C}{N_c}\sum_{\substack{\mathbf{k}\mathbf{k}',ll'\\ \sigma\sigma',\xi\xi'}}\gamma^\dagger_{\mathbf{k}l\sigma\xi}\gamma_{\mathbf{k}'l\sigma\xi}\gamma^\dagger_{\mathbf{k}'l'\sigma'\xi'}\gamma_{\mathbf{k}l'\sigma'\xi'}, \quad (5)$$

where N_c is the number of unit cells in the sample, and V_C is an effective interaction constant whose value can be potentially extracted from the low-temperature data[25–34] on spontaneous symmetry breaking in AB-BLG. The forward scattering is characterized by a small momentum transfer $|\mathbf{k}-\mathbf{k}'| \ll |\mathbf{K}_1 - \mathbf{K}_2|$, and preserves the band indices l and l' of the two participating electrons. Next, one can define the backscattering term

$$H^{\rm b}_{\rm int} = \frac{V^{\rm b}_C}{N_c}\sum_{\substack{\mathbf{k}\mathbf{k}',ll'\\ \sigma\sigma',\xi}}\gamma^\dagger_{\mathbf{k}l\sigma\xi}\gamma_{\mathbf{k}'l\sigma\bar\xi}\gamma^\dagger_{\mathbf{k}'l'\sigma'\bar\xi}\gamma_{\mathbf{k}l'\sigma'\xi}, \quad (6)$$

where a bar on top of a binary-valued index implies the inversion of the index value (for example, if $\xi = 1$ then $\bar\xi = -1$). For $H^{\rm b}_{\rm int}$ the transferred momentum is large $|\mathbf{k}-\mathbf{k}'| \sim |\mathbf{K}_1 - \mathbf{K}_2|$, thus we can assume that $V^{\rm b}_C \ll V_C$. Finally, the umklapp-type interaction

$$H^{\rm u}_{\rm int} = \frac{V^{\rm u}_C}{N_c}\sum_{\substack{\mathbf{k}\mathbf{k}',\\ \sigma\sigma',\xi\xi'}}\gamma^\dagger_{\mathbf{k}1\sigma\xi}\gamma_{\mathbf{k}'2\sigma\xi}\gamma^\dagger_{\mathbf{k}'1\sigma'\xi'}\gamma_{\mathbf{k}2\sigma'\xi'} + \text{h.c.}, \quad (7)$$

represents scattering events in which both electrons change their bands. It accounts for the coupling between inter-layer dipole moments, which is also weaker than the coupling between charge densities represented by $H^{\rm f}_{\rm int}$. In principle, there is backscattering umklapp, which we do not consider due to it being even weaker than $H^{\rm u}_{\rm int}$.

III. MEAN-FIELD APPROXIMATION

We consider a zero-temperature SDW instability of the AB-BLG. This is characterized by the spontaneous generation of staggered spin magnetization violating the spin-rotation symmetry. The direction of this magnetization is not fixed and there are several equivalent choices for an SDW order parameter that differ by the spin-magnetization direction. It is convenient to assume that $\langle\gamma^\dagger_{\mathbf{k}1\sigma\xi}\gamma_{\mathbf{k}2\bar\sigma\xi}\rangle \neq 0$. This choice corresponds to the magnetization in the xy-plane. Note also that the introduced order parameter accounts for the coupling of single-electron states in the same valley ξ.

Now, assuming that the backscattering (6) and the umklapp (7) are weak, we apply the mean-field approximation to $H^{\rm f}_{\rm int}$

$$H^{\rm MF}_{\rm int} = -\sum_{\mathbf{k}\sigma\xi}\Delta_{\sigma\xi}\gamma^\dagger_{\mathbf{k}2\sigma\xi}\gamma_{\mathbf{k}1\bar\sigma\xi} + \text{h.c.} + B, \quad (8)$$

where the order parameter $\Delta_{\sigma\xi}$ and c-number B are

$$\Delta_{\sigma\xi} = \frac{V_C}{N_c}\sum_{\mathbf{q}}\langle\gamma^\dagger_{\mathbf{q}1\sigma\xi}\gamma_{\mathbf{q}2\bar\sigma\xi}\rangle\Theta(q_C - q), \quad (9)$$

$$B = \sum_{\mathbf{q}\sigma\xi}\Delta_{\sigma\xi}\langle\gamma^\dagger_{\mathbf{q}2\sigma\xi}\gamma_{\mathbf{q}1\bar\sigma\xi}\rangle\Theta(q_C - q) = \frac{N_c}{V_C}\sum_{\sigma\xi}|\Delta_{\sigma\xi}|^2. \quad (10)$$

In these expressions, the momentum cutoff for the interaction q_C satisfies $q_C \ll |\mathbf{K}_1 - \mathbf{K}_2|$.

The mean-field Hamiltonian (8) does not conserve spin (spin-rotation symmetry is spontaneously broken for non-zero $\Delta_{\sigma\xi}$). However, quasi-momentum $\mathbf{q}$ is conserved. In addition to $\mathbf{q}$, one can introduce valley and spin-flavor operators

$$S^{\rm f}_{\mathbf{q}} = \sum_{\sigma\xi l}(-1)^{l+1}\sigma\gamma^\dagger_{\mathbf{q}l\sigma\xi}\gamma_{\mathbf{q}l\sigma\xi}, \quad S^{\rm v}_{\mathbf{q}} = \sum_{\sigma\xi l}\xi\gamma^\dagger_{\mathbf{q}l\sigma\xi}\gamma_{\mathbf{q}l\sigma\xi}, \quad (11)$$

which commute with the Hamiltonian $H_0 + H^{\rm MF}_{\rm int}$ and are good quantum numbers. Thus, in this approximation all fermionic degrees of freedom can be grouped into four uncoupled sectors, each sector having its own values of

spin-flavor index $(-1)^{l+1}\sigma$ and valley index ξ. A sector is characterized by its own order parameter $\Delta_{\sigma\xi}$, and single-particle spectrum

$$E^{1,2}_{\mathbf{q}\sigma\xi} = \pm\sqrt{\Delta^2_{\sigma\xi} + \left(\frac{\hbar^2 v_{\rm F}^2}{t_0}\right)^2 q^4}. \quad (12)$$

The thermodynamic grand potential Ω can be expressed as a sum

$$\Omega = \sum_{\sigma\xi} \Omega_{\sigma\xi} + B, \quad (13)$$

where $\Omega_{\sigma\xi}$ are four partial grand potentials corresponding to specific sectors. At zero temperature, these are

$$\Omega_{\sigma\xi} = \sum_{\mathbf{q}l} \left(E^l_{\mathbf{q}\sigma\xi} - \mu\right) \Theta\left(\mu - E^l_{\mathbf{q}\sigma\xi}\right), \quad (14)$$

where μ is the chemical potential.

Minimization of Ω over the order parameters allows us to derive the following independent self-consistency equations for the order parameters in the four sectors

$$1 = \frac{V_C}{N_c} \sum_{|\mathbf{q}|<q_C} \frac{\Theta(\mu + E^1_{\mathbf{q}\sigma\xi}) - \Theta(\mu - E^1_{\mathbf{q}\sigma\xi})}{E^1_{\mathbf{q}\sigma\xi}}. \quad (15)$$

Since the model is electron-hole symmetric, we can limit our discussion to the $\mu > 0$ case only. For positive chemical potential: $\Theta(\mu + E^1_{\mathbf{q}\sigma}) - \Theta(\mu - E^1_{\mathbf{q}\sigma}) = \Theta(E^1_{\mathbf{q}\sigma} - \mu)$. Introducing dimensionless variables

$$g = \frac{V_C t_0}{\sqrt{3}\pi t^2},\ m = \frac{4t_0\mu}{9t^2},\ \delta_{\sigma\xi} = \frac{4t_0\Delta_{\sigma\xi}}{9t^2}, \quad (16)$$

we obtain from Eq. (15)

$$1 = 2g \int_{Q^m_{\sigma\xi}}^{Q_C} \frac{QdQ}{\sqrt{\delta^2_{\sigma\xi} + Q^4}}, \quad (17)$$

where

$$Q_C = a_0 q_C, \quad Q^m_{\sigma\xi} = (m^2 - \delta^2_{\sigma\xi})^{1/4}. \quad (18)$$

It is evident that the gap in the spectrum of electrons in the sector (σ, ξ) arises only if $Q_C > Q^m_{\sigma\xi}$, that is, if the number of the doped charge carriers in this sector is not too large. One can perform the integration in Eq. (17) and obtain that

$$1 = g \ln\left(\frac{Q_C^2 + \sqrt{\delta^2_{\sigma\xi} + Q_C^4}}{m + \sqrt{m^2 - \delta^2_{\sigma\xi}}}\right). \quad (19)$$

In the weak coupling limit, $g \ll 1$, we have $\delta_{\sigma\xi} \ll Q_C^2$. Consequently

$$\Delta_{\sigma\xi} = \sqrt{\Delta_0(2\mu - \Delta_0)}, \quad (20)$$

where

$$\Delta_0 = \frac{9t^2}{4t_0} q_C^2 a_0^2 e^{-1/g} \quad (21)$$

is the mean-field gap of undoped AB-BLG. Further defining

$$\delta_0 = \frac{4t_0\Delta_0}{9t^2}, \quad (22)$$

we can express Eq. (20) in dimensionless form

$$\delta_{\sigma\xi} = \sqrt{\delta_0(2m - \delta_0)}. \quad (23)$$

For finite doping, Eq. (20) implies that the chemical potential must satisfy $\mu \geq \Delta_{\sigma\xi}$. Such a relation is naturally expected: to start doping, the chemical potential must exceed the gap.

Since experiments are performed at fixed doping, we need to connect the values of $\Delta_{\sigma\xi}$ with doping. It is convenient to introduce partial doping, that is, the number of electrons with specific values of $(-1)^{l+1}\sigma$ and ξ:

$$x_{\sigma\xi} = -\frac{\partial\Omega_{\sigma\xi}}{\partial\mu} = \frac{2\pi}{V_{\rm BZ}} \sum_{\sigma\xi} \int kdk\Theta(\mu - E^1_{\mathbf{k}\sigma\xi}). \quad (24)$$

The total doping x is equal to

$$x = \sum_{\sigma\xi} x_{\sigma\xi}. \quad (25)$$

If $\mu > \Delta_{\sigma\xi}$, we obtain the relation between the partial doping and the chemical potential in the form

$$x_{\sigma\xi} = \frac{3\sqrt{3}}{8\pi}\sqrt{m^2 - \delta^2_{\sigma\xi}}. \quad (26)$$

Otherwise, $x_{\sigma\xi} = 0$. As a result, we derive in the case of non-zero $x_{\sigma\xi}$

$$m = \delta_0 - \frac{8\pi}{3\sqrt{3}} x_{\sigma\xi} = \delta_0\left(1 - \frac{2x_{\sigma\xi}}{x_0}\right), \quad (27)$$

$$\delta_{\sigma\xi} = \delta_0\sqrt{1 - \frac{4x_{\sigma\xi}}{x_0}}, \quad (28)$$

where

$$x_0 = \frac{t_0\Delta_0}{\sqrt{3}\pi t^2}. \quad (29)$$

Equation (28) indicates that for $x_{\sigma\xi} = x_0/4$ the order parameter in the sector vanishes. That is, for $x_{\sigma\xi} > x_0/4$ one has

$$\Delta_{\sigma\xi}(x_{\sigma\xi}) \equiv 0, \quad m = \frac{8\pi}{3\sqrt{3}} x_{\sigma\xi} = \frac{2\delta_0}{x_0} x_{\sigma\xi}. \quad (30)$$

Note that the chemical potential, as given by Eqs. (27) and (30), demonstrates non-monotonic behavior as a function of $x_{\sigma\xi}$. Of particular importance is the fact that, for low doping, $\mu = \mu(x_{\sigma\xi})$ is a decreasing function. This means that the compressibility of the homogeneous phase is negative and points to a possibility of the phase separation of the electronic liquid. We will assume below that the long-range Coulomb interaction is sufficiently strong to arrest the phase separation, restoring the stability of homogeneous states.

IV. QUARTER METAL STATE OF DOPED AB-BLG

Disregarding the possibility of the phase separation, we use Eqs. (27) and (28) to characterize the thermodynamics of the system. To describe the doped state of the electronic liquid for a specific x, one must determine partial dopings in all four sectors. To achieve this goal, we calculate the free energy

$$F(x) = F(0) + \sum_{\sigma\xi} \delta F(x_{\sigma\xi}). \tag{31}$$

In this formula $F(0)$ is the free energy of the undoped system, and $\delta F(x_{\sigma\xi})$ shows how much the sector (σ, ξ) contributes, for given partial doping $x_{\sigma\xi}$, to the total free energy $F(x)$. The contribution $\delta F(x_{\sigma\xi})$ can be found with the help of the relation

$$\delta F(x_{\sigma\xi}) = \int_0^{x_{\sigma\xi}} \mu(x')dx', \tag{32}$$

and Eq. (27) and (30) that connect the chemical potential and partial doping. Thus we derive

$$\delta F(x_{\sigma\xi}) = \begin{cases} \Delta_0 \left(x_{\sigma\xi} - \frac{x_{\sigma\xi}^2}{x_0} \right), & \text{if } 0 \le x_{\sigma\xi} \le \frac{x_0}{4}, \\ \Delta_0 \left(\frac{x_0}{8} + \frac{x_{\sigma\xi}^2}{x_0} \right), & \text{if } x_{\sigma\xi} > \frac{x_0}{4}. \end{cases} \tag{33}$$

The free energy (31) must be minimized over $x_{\sigma\xi}$ under the constraint (25).

For a generic value of x, the particulars of such a minimization procedure might be somewhat cumbersome. Yet for small doping $x < x_0/4$, calculations simplify significantly due to all partial dopings being limited by $x_0/4$ from above. In this regime one can demonstrate that F is smallest when all charges are placed into a single sector

$$x_{\sigma\xi} = x, \quad x_{\sigma'\xi'} = 0, \text{ for } \sigma' \neq \sigma \text{ or } \xi' \neq \xi. \tag{34}$$

For the distribution (34), the doping-dependent part of the free energy equals to

$$F_{\rm QM} = \Delta_0 \left(x - \frac{x^2}{x_0} \right). \tag{35}$$

It is smaller, for example, than the free energy

$$F_{\rm eq} = \Delta_0 \left(x - \frac{x^2}{4x_0} \right) \tag{36}$$

calculated for an equal distribution of doping between all four sectors ($x_{\sigma\xi} = x/4$ for all σ and ξ).

The state described by Eq. (34) is metallic, with (almost) circular Fermi surface whose radius $k_{\rm F} = k_{\rm F}(x)$ is set by the equation

$$a_0^2 k_{\rm F}^2 = \frac{8\pi x}{3\sqrt{3}}. \tag{37}$$

This Fermi surface, however, is quite unique: all single-electronic states reaching the Fermi energy are perfectly polarized in terms of $S^{\rm f}$ and $S^{\rm v}$. In other words, they have an identical value of $(-1)^{l+1}\sigma$, and the Fermi surface is located within a single valley $\mathbf{K}_\xi$. Since among four possible Fermi surface sheets of the non-interacting theory, only one sheet emerges in the system, it is natural to designate such a conducting state as a QM. To appreciate the difference between a metal with equal distribution of charges between the sectors on one side and a QM on the other side, one can compare pages (a) and (b) of Fig. 1.

V. CASCADE OF PHASE TRANSITION BETWEEN DIFFERENT SYMMETRY-BROKEN PHASES

The QM state described above remains stable only for sufficiently low x: one sector cannot accommodate too much doping. Indeed, when $x = x_0/2$, Eq. (30) implies that $\mu = \Delta_0$. Doping a single sector beyond this point is impossible: adding more charge to this sector increases the chemical potential beyond Δ_0, unavoidably placing charges into the remaining sectors as well. As a result, a cascade of doping-driven phase transitions emerges. The transitions connect different metallic states, each state being characterized by a number of doped sectors: 1, 2, 3, or 4 [paramagnetic (PM) state] sectors.

Let us briefly describe this cascade of transitions (see Figs. 1 and 2). At zero doping the system is gapped with the gap equal to Δ_0 in all sectors. For small x, the system absorbs all extra charge carriers into a single sector [say, sector ($\sigma = \uparrow$, $\xi = +1$)]. This is a QM state [Fig. 1(b)]. The order parameter in this sector gradually decreases with doping. At the same time, the chemical potential decreases with doping indicating the possibility of the phase separation. However, we assume that the long-range Coulomb repulsion totally arrests the phase separation and the electronic state remains homogeneous. At $x = x_0/4$, the order parameter in doped sector vanishes, and a second order phase transition inside the QM state takes place. This transition is characterized by the complex order parameter and a presence of the developed Fermi surface.

Beyond $x = x_0/4$, order parameter $\Delta_{\uparrow+1}$ is zero. Yet, the QM state remains stable for $x < x_0/2$. At higher doping, the extra charge comes to some other sector [for definiteness, we assign this to be ($\sigma = \uparrow$, $\xi = -1$); other configurations are equiprobable]. However, one can show that the state when the order parameter of this sector is greater than 0 but less than Δ_0 is metastable one. The stable state corresponds to $\Delta_{\uparrow-1} = 0$. As a result, there appears a first order phase transition between QM state with $\Delta_{\uparrow+1} = 0$ (other sectors are gapped) and HM state with $\Delta_{\uparrow+1} = \Delta_{\uparrow-1} = 0$ (other sectors are gapped) [Fig. 1(c)]. It happens at $x = x_0/2$. This critical doping is found by comparison of the free energies of corresponding states.

As x increases further, one reaches the point where the HM energy becomes equal to that of a 3/4 metal

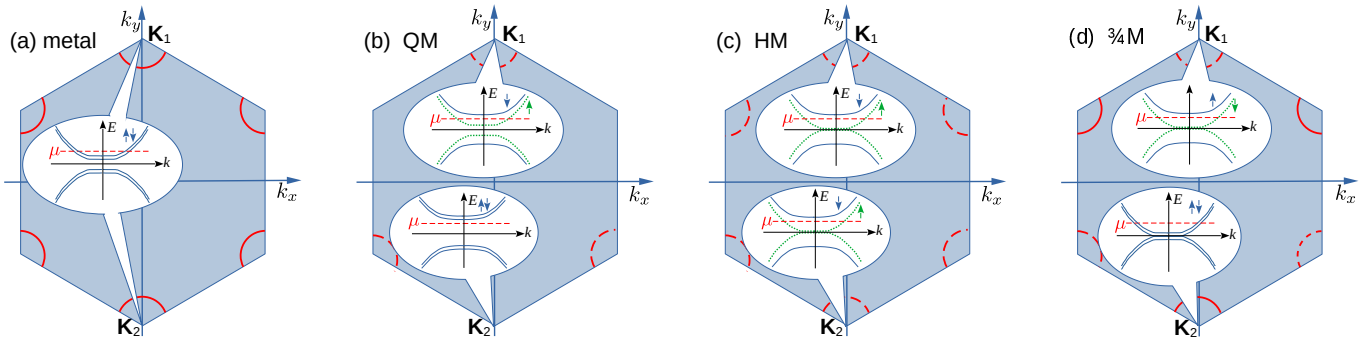

FIG. 1. Fermi surface structure of different metallic states. Filled (blue) hexagon is the Brillouin zone of AB-BLG. Dirac points $\mathbf{K}_{1,2}$ are marked. Solid and dashed (red) arks near the Dirac points are the Fermi surface segments. The segments with double degeneracy over the spin-flavor index are shown as solid curves. Non-degenerate Fermi surface sheets are represented by dashed arcs. Diagrams inside callouts depict schematically the quasiparticle dispersion near a specific Dirac point. Horizontal (red) dashed line represents chemical potential level. Degenerate bands are shown by solid (blue) double curves. When this degeneracy is lifted, as in panels (b), (c), and (d), the bands touching or moving closer to one another, are plotted by dotted (green) curve. Vertical arrows represent the spin-flavor index $(-1)^{l+1}\sigma$. Ordinary metallic state in panel (a) has a Fermi surface sheet in both valleys. However, within framework of our model, its energy is higher than the energy of FraM states (at fixed doping). Panel (b) depicts the quarter-metal phase, which is stable at not-too-large doping. For this state, the available Fermi surface is located in one valley only, and is non-degenerate. Note that QM is nematic (violates rotation symmetry). A specific example of a half-metal state is shown in panel (c). Here the Fermi surface is present in both valleys, but it is non-degenerate. Panel (d) corresponds to 3/4-metal. The Fermi surface is in both valleys, however, in one valley the Fermi surface sheet is degenerate, in the other it is not. Because of this, this phase is nematic.

($\frac{3}{4}$M) state [Fig. 1(d)]. In such a state, three sectors [say, ($\sigma =\uparrow, \xi = +1$), ($\sigma =\uparrow, \xi = -1$), and ($\sigma =\downarrow, \xi = +1$)] are doped, and the fourth sector, ($\sigma =\downarrow, \xi = -1$), is gapped, with the extra charge carriers being equally distributed among the three doped sectors. Again, one can show that the state corresponding to $0 < \Delta_{\downarrow+1} < \Delta_0$ is metastable one. In the stable $\frac{3}{4}$M state the order parameters in all three doped sectors vanish. As a result, there appears a first order phase transition between HM and $\frac{3}{4}$M states. Comparing the free energies of these two states, one finds the point of the transition. It appears at $x = \sqrt{3/4}x_0$.

If doping is continued even further, the $\frac{3}{4}$M state is replaced by the PM state [Fig. 1(a)]. This is yet another first-order transition, and the last one in the transition cascade. It occurs at $x = \sqrt{3/2}x_0$. The value of this doping is found by comparison of the free energies of $\frac{3}{4}$M and PM states. The phase diagram of the system is shown in Fig. 2. In this figure only the electron doping is shown. Due to electron-hole symmetry of our model, the phase diagram at hole doping is equivalent to that shown in Fig. 2 up to the replacement $x \to -x$.

VI. DISCUSSION

We would like to stress here several important points. One must remember that the HM state realized in our model upon sufficiently strong doping is not the conventional HM[1,2] whose Fermi surface demonstrates perfect spin polarization. Instead, we now have a spin-flavor HM[35–38], with perfect spin-flavor polarization of the Fermi surface. This means that the electron (hole) single-particle states reaching the Fermi energy have their spin projection being equal to σ (to $\bar{\sigma}$). (The related feature of the QM state was already mentioned above.) In a model with electron-hole symmetry a spin-flavor-polarized FraM state does not accumulate net spin polarization. However, a finite spin polarization may accompany a finite spin-flavor polarization[35] when such a symmetry is absent. The spin polarization was indeed observed in Ref. 16.

We argued above that the relative stability of various metallic states is affected by doping, triggering the transitions between them. Doping is not, however, the only factor that influence the competition between the FraM phases. Particular model's ingredients favoring HM states are the umklapp and backscattering interaction terms. Specifically, the umklapp couples two sectors with unequal $(-1)^l\sigma$, the backscattering, on the other hand, connect the sectors with non-identical values of the ξ index. Thus, in the presence of either strong $H^{\rm u}_{\rm int}$ or strong $H^{\rm b}_{\rm int}$ only two (not four) decoupled sectors of the mean-field Hamiltonian can be defined, promoting the HM phase over other FraM's. Therefore, in more realistic models, the critical doping values are no longer proportional to x_0, with universal proportionality coefficients. Instead, they become functions of the backscattering and umklapp coupling constants. Finally, one must remember that our single-electron Hamiltonian is based on the simplest effective model of AB-BLG. It unavoidably ignores some details of the AB-BLG band structure, such as the trigonal warping caused by a longer-range hopping terms[17,18]. Specifically, the trigonal warping acts to replace the parabolic dispersion of the Hamiltonian (2)

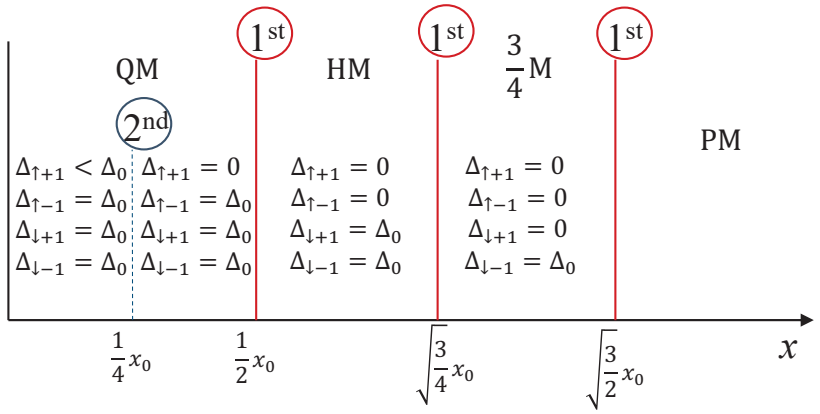

FIG. 2. Cascade of the doping-driven phase transitions between different FraM states with different valley and/or spin-flavor (isospin) polarizations. Only the region of electron doping is shown. For hole doping the picture is identical up to a replacement $x \to -x$. Vertical solid (dashed) lines represent first (second) order transitions.

with four Dirac cones, depleting the density of states at the Dirac points. The latter, in turn, reduces the transition temperature, making the transition itself even more dependent on the strength of the interaction. Fortunately, there is ample experimental evidence suggesting that electron-electron interaction in AB-BLG is sufficiently strong to cause low-temperature ordering. Thus, as the simple approximation, these band effects can be ignored, and Hamiltonian (2) can be used. Yet, for more detailed modeling of the transition cascade a more accurate band description is necessary.

The qualitative agreement between the remarkable recent experiments reported in Ref. 16 and our formalism is very encouraging. The proposed theory can account for such experimentally observed features as the cascade of phase transitions, magnetization, and valley polarizations. Yet one must keep in mind that the experiments were performed at finite electric field applied transverse to a sample. In our formalism, this field is assumed to be zero. Further research is needed to understand the role of this field.

To conclude, we proposed a mechanism responsible for the formation of the FraM states in doped AB-BLG. We argue that, as doping increases, this system demonstrates a cascade of phase transitions between various metallic phases that differ in terms of spin-flavor and valley polarizations of their Fermi surfaces. Our theoretical findings compare favorably to very recent experiments[16] on AB-BLG.

[1] R. A. de Groot, F. M. Mueller, P. G. van Engen, and K. H. J. Buschow, "New Class of Materials: Half-Metallic Ferromagnets," Phys. Rev. Lett. **50**, 2024 (1983).

[2] M. I. Katsnelson, V. Y. Irkhin, L. Chioncel, A. I. Lichtenstein, and R. A. de Groot, "Half-metallic ferromagnets: From band structure to many-body effects," Rev. Mod. Phys. **80**, 315 (2008).

[3] X. Hu, "Half-Metallic Antiferromagnet as a Prospective Material for Spintronics," Adv. Mater. **24**, 294 (2012).

[4] K. E. H. M. Hanssen, P. E. Mijnarends, L. P. L. M. Rabou, and K. H. J. Buschow, "Positron-annihilation study of the half-metallic ferromagnet NiMnSb: Experiment," Phys. Rev. B **42**, 1533 (1990).

[5] J.-H. Park, E. Vescovo, H.-J. Kim, C. Kwon, R. Ramesh, and T. Venkatesan, "Direct evidence for a half-metallic ferromagnet," Nature **392**, 794 (1998).

[6] Y. Ji, G. J. Strijkers, F. Y. Yang, C. L. Chien, J. M. Byers, A. Anguelouch, G. Xiao, and A. Gupta, "Determination of the Spin Polarization of Half-Metallic CrO_2 by Point Contact Andreev Reflection," Phys. Rev. Lett. **86**, 5585 (2001).

[7] M. Jourdan, J. Minár, J. Braun, A. Kronenberg, S. Chadov, B. Balke, A. Gloskovskii, M. Kolbe, H. Elmers, G. Schönhense, et al., "Direct observation of half-metallicity in the Heusler compound Co_2MnSi," Nat. Commun. **5**, 3974 (2014).

[8] A. Du, S. Sanvito, and S. C. Smith, "First-Principles Prediction of Metal-Free Magnetism and Intrinsic Half-Metallicity in Graphitic Carbon Nitride," Phys. Rev. Lett. **108**, 197207 (2012).

[9] A. Hashmi and J. Hong, "Metal free half metallicity in 2D system: structural and magnetic properties of g-C_4N_3 on BN," Sci. Rep. **4**, 4374 (2014).

[10] Y.-W. Son, M. L. Cohen, and S. G. Louie, "Half-metallic graphene nanoribbons," Nature **444**, 347 (2006).

[11] E. Kan, W. Hu, C. Xiao, R. Lu, K. Deng, J. Yang, and H. Su, "Half-metallicity in organic single porous sheets," J. Am. Chem. Soc. **134**, 5718 (2012).

[12] B. Huang, C. Si, H. Lee, L. Zhao, J. Wu, B.-L. Gu, and W. Duan, "Intrinsic half-metallic BN–C nanotubes," Appl. Phys. Lett. **97**, 043115 (2010).

[13] I. Žutić, J. Fabian, and S. Das Sarma, "Spintronics: Fundamentals and applications," Rev. Mod. Phys. **76**, 323 (2004).

[14] A. O. Sboychakov, A. L. Rakhmanov, A. V. Rozhkov, and F. Nori, "Bilayer graphene can become a fractional metal," Phys. Rev. B **103**, L081106 (2021).

[15] H. Zhou, T. Xie, A. Ghazaryan, T. Holder, J. R. Ehrets, E. M. Spanton, T. Taniguchi, K. Watanabe, E. Berg, M. Serbyn, et al., "Half- and quarter-metals in rhombohedral trilayer graphene," Nature **598**, 429 (2021).

[16] de la Barrera, C. Sergio, S. Aronson, Z. Zheng, K. Watanabe, T. Taniguchi, Q. Ma, P. Jarillo-Herrero, and R. Ashoori, "Cascade of isospin phase transitions in Bernal-stacked bilayer graphene at zero magnetic field," Nature Physics **18**, 771 (2022).

[17] E. McCann and V. I. Fal'ko, "Landau-Level Degeneracy and Quantum Hall Effect in a Graphite Bilayer," Phys. Rev. Lett. **96**, 086805 (2006).

[18] J. Jung and A. H. MacDonald, "Accurate tight-binding models for the π bands of bilayer graphene," Phys. Rev. B **89**, 035405 (2014).

[19] A. Rozhkov, A. Sboychakov, A. Rakhmanov, and F. Nori, "Electronic properties of graphene-based bilayer systems," Phys. Rep. **648**, 1 (2016).

[20] E. H. Hwang and S. Das Sarma, "Screening, Kohn Anomaly, Friedel Oscillation, and RKKY Interaction in Bilayer Graphene," Phys. Rev. Lett. **101**, 156802 (2008).

[21] Y. Lemonik, I. Aleiner, and V. I. Fal'ko, "Competing nematic, antiferromagnetic, and spin-flux orders in the ground state of bilayer graphene," Phys. Rev. B **85**, 245451 (2012).

[22] O. Vafek, "Interacting fermions on the honeycomb bilayer: From weak to strong coupling," Phys. Rev. B **82**, 205106 (2010).

[23] O. Vafek and K. Yang, "Many-body instability of Coulomb interacting bilayer graphene: Renormalization group approach," Phys. Rev. B **81**, 041401 (2010).

[24] V. Cvetkovic, R. E. Throckmorton, and O. Vafek, "Electronic multicriticality in bilayer graphene," Phys. Rev. B **86**, 075467 (2012).

[25] B. E. Feldman, J. Martin, and A. Yacoby, "Broken-symmetry states and divergent resistance in suspended bilayer graphene," Nat. Phys. **5**, 889 (2009).

[26] J. Martin, B. E. Feldman, R. T. Weitz, M. T. Allen, and A. Yacoby, "Local Compressibility Measurements of Correlated States in Suspended Bilayer Graphene," Phys. Rev. Lett. **105**, 256806 (2010).

[27] R. T. Weitz, M. T. Allen, B. E. Feldman, J. Martin, and A. Yacoby, "Broken-Symmetry States in Doubly Gated Suspended Bilayer Graphene," Science **330**, 812 (2010).

[28] A. S. Mayorov, D. C. Elias, M. Mucha-Kruczynski, R. V. Gorbachev, T. Tudorovskiy, A. Zhukov, S. V. Morozov, M. I. Katsnelson, V. I. Fal'ko, A. K. Geim, et al., "Interaction-Driven Spectrum Reconstruction in Bilayer Graphene," Science **333**, 860 (2011).

[29] W. Bao, J. Velasco, F. Zhang, L. Jing, B. Standley, D. Smirnov, M. Bockrath, A. H. MacDonald, and C. N. Lau, "Evidence for a spontaneous gapped state in ultraclean bilayer graphene," PNAS **109**, 10802 (2012).

[30] F. Freitag, J. Trbovic, M. Weiss, and C. Schönenberger, "Spontaneously Gapped Ground State in Suspended Bilayer Graphene," Phys. Rev. Lett. **108**, 076602 (2012).

[31] F. Freitag, M. Weiss, R. Maurand, J. Trbovic, and C. Schönenberger, "Homogeneity of bilayer graphene," Solid State Communications **152**, 2053 (2012).

[32] J. Velasco Jr., L. Jing, W. Bao, Y. Lee, P. Kratz, V. Aji, M. Bockrath, C. Lau, C. Varma, R. Stillwell, et al., "Transport spectroscopy of symmetry-broken insulating states in bilayer graphene," Nat. Nanotechnol. **7**, 156 (2012).

[33] A. Veligura, H. J. van Elferen, N. Tombros, J. C. Maan, U. Zeitler, and B. J. van Wees, "Transport gap in suspended bilayer graphene at zero magnetic field," Phys. Rev. B **85**, 155412 (2012).

[34] F. Freitag, M. Weiss, R. Maurand, J. Trbovic, and C. Schönenberger, "Spin symmetry of the bilayer graphene ground state," Phys. Rev. B **87**, 161402 (2013).

[35] A. V. Rozhkov, A. L. Rakhmanov, A. O. Sboychakov, K. I. Kugel, and F. Nori, "Spin-Valley Half-Metal as a Prospective Material for Spin Valleytronics," Phys. Rev. Lett. **119**, 107601 (2017).

[36] A. L. Rakhmanov, A. O. Sboychakov, K. I. Kugel, A. V. Rozhkov, and F. Nori, "Spin-valley half-metal in systems with Fermi surface nesting," Phys. Rev. B **98**, 155141 (2018).

[37] A. V. Rozhkov, A. O. Sboychakov, D. A. Khokhlov, A. L. Rakhmanov, and K. I. Kugel, "New half-metallic states in systems with spin and charge density wave," Pis'ma v ZhETF **112**, 764 (2020) [JETP Lett. **112**, 725 (2020)].

[38] D. A. Khokhlov, A. L. Rakhmanov, A. V. Rozhkov, and A. O. Sboychakov, "Dynamical spin susceptibility of a spin-valley half-metal," Phys. Rev. B **101**, 235141 (2020).